CIRCULATORY PATTERNS OF AIR POLLUTANTS WITHIN THE BARCELONA AIR BASIN IN A SUMMERTIME SITUATION: LIDAR AND NUMERICAL APPROACHES

CECILIA SORIANO[1], JOSÉ M. BALDASANO[1], WILLIAM T. BUTTLER[2] and KURT R. MOORE[3]

[1]*Laboratory of Environmental Modeling DPE-ETSEIB, Universitat Politècnica de Catalunya (UPC), Av. Diagonal 647,10.24. 08028 Barcelona, Spain;* [2]*Los Alamos National Laboratory (LANL), Physics Division (P-22), MS H803, Los Alamos, NM 87545, U.S.A.;* [3]*Los Alamos National Laboratory (LANL), Non-Proliferation and International Securities-1 (NIS-1), MS D466, Los Alamos, NM 87545, U.S.A.*

(Received in final form 11 May 2000)

Abstract. This work examines circulatory patterns of air pollutants in the area of Barcelona (Spain), a region with strong coastal and orographic influences. This was achieved through exploitation of elastic-backscatter lidar data and by numerical simulation of the atmosphere with a meteorological mesoscale model (MEMO). Lidar data were acquired in July 1992 during a collaborative campaign between Los Alamos National Laboratory (LANL) and the Polytechnic University of Catalonia (UPC). The lidar provided information about the distribution of aerosols and the prevailing winds, determined by application of a maximum cross-correlation algorithm to elastic-backscatter lidar data. Lidar winds are used to evaluate high altitude winds simulated by the model. This study showed that circulatory patterns in Barcelona are correlated with daytime convective vertical mixing, sea-breeze circulations, and vertical forcing caused by mountain thermal and mechanical effects.

Keywords: Elastic-backscatter lidar, Lidar, Mesoscale meteorology, Numerical modeling.

1. Introduction

Understanding the main circulatory patterns of air pollutants within a study region is required for regional air-quality studies. Mesoscale circulatory patterns are mainly determined by the orography of the region; orographic variations are the primary cause of the non-universality of air-quality management at the regional scale. Remediation methods must thus be designed for the unique orographic qualities of a region.

Most mesoscale air-quality studies combine measurement of variables that influence the establishment of mesoscale circulations with numerical simulations from meteorological and dispersion models to determine the evolution of air pollutant concentrations. Variables of interest include: pollutant emissions, air pollution concentration and meteorological variables that play an important role in pollutant dispersion (such as wind speed and direction, and the atmospheric temperature profile). These two methodologies are complimentary. For example, measurements are

Boundary-Layer Meteorology **98:** 33–55, 2001.

needed to provide model initialization parameters and allow for later performance evaluation. Moreover, the utility of a model is its ability to provide a spatial and temporal resolution unachievable with classical meteorological observational techniques, such as networked surface stations and vertical soundings with balloons and radiosondes.

Recently, advances in lidar techniques have shown lidar to be a useful tool for regional pollution observations in regions of complex orography. Lidar provides a capability to remotely determine vector (three-dimensional winds) and scalar (elastic backscatter) fields at a high resolution, approaching that of meteorological models. For example, vertical scans from elastic-backscatter lidar show the distribution of aerosols within the atmosphere and can be used to infer patterns of air pollutant circulation (Johnson, 1969; Wakimoto and McElroy, 1986; Baldasano et al., 1994a; Hoff et al., 1997). The latter capability follows as aerosols trace motions within the atmosphere.

Because of its high spatial and temporal resolution, lidar can play an important role in the task of assessing model performance. The usual method used to evaluate a model is by comparison with data from surface (point) stations. The primary drawback of this type of comparison is that mesoscale models cannot simulate local features near a surface station, features that may influence local measurements provided by surface stations.

Remote lidar techniques allow for the evaluation of models at higher altitudes by providing wind information at levels where surface perturbations are minimized (Soriano, 1997). For these reasons, we have combined lidar techniques with meteorological simulations to describe the circulatory patterns of air pollutants in the Barcelona area. Other studies in the Barcelona region (Baldasano et al., 1994b; Calbó and Baldasano, 1995) have implemented meteorological models. However, this study also includes results from the first measurements ever made in Barcelona with a lidar device.

2. Description of the Barcelona Area

Barcelona is located on the shores of the Mediterranean Sea, on the northeastern corner of the Iberian Peninsula. Its location, together with the orography surrounding the region, contributes to the complexity of the dispersion of pollutants emitted in the region. The study models a region centered on the city of Barcelona and covering an area of 80×80 km^2 (Figure 1). The figure also shows the position of the lidar during the experimental campaign, at 285 m above sea level.

The lidar only monitored a domain covering approximately 40 km^2 above the city of Barcelona (its maximum range was 7 km). However, a larger simulation domain was chosen because earlier studies (Baldasano et al., 1994b; Calbó and Baldasano, 1995) indicated that it contains most of the orographic features driving the wind patterns in the area. The orography of the region is dominated by

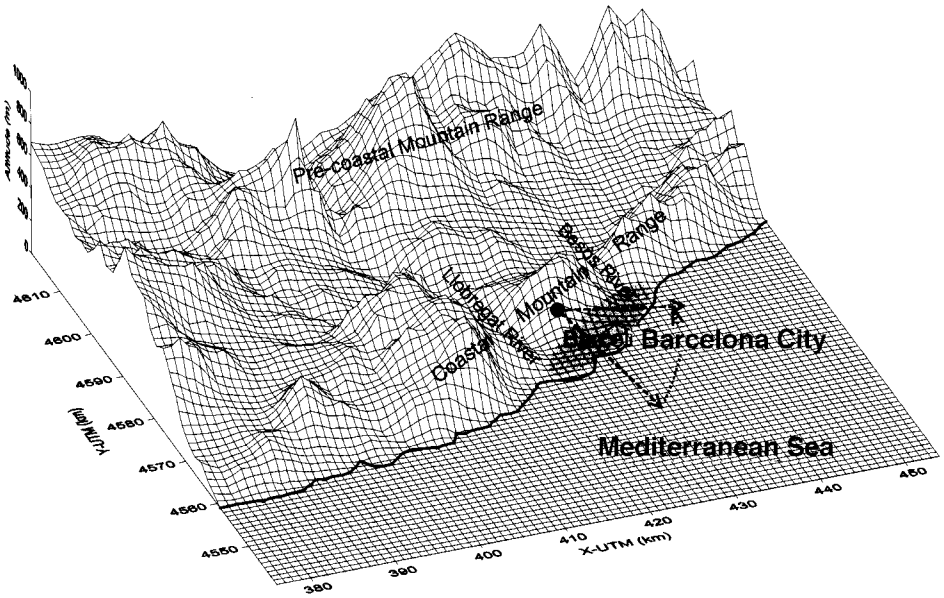

Figure 1. The Barcelona Geographical Area. Dot marks lidar position during the experimental campaign of July 1992, and the dotted lines show the direction along which the vertical scans of Figure 2 were acquired. The shaded area shows the location of the city of Barcelona within the region.

four main features arranged parallel to the coastline: (1) the coastal plain, which comprises an 8-km strip of land between the sea and the first mountain range and which includes most of the cities in the greater urban area of Barcelona; (2) the coastal mountain range with altitudes between 250 and 512 m; (3) the pre-coastal depression, situated between the coastal mountain range; and (4) the pre-coastal mountain range, with maximum altitudes of $\approx$1500 m.

Note that there are two main river valleys in the area: Llobregat and Besòs. These rivers frame the city and their respective valleys play an important role in the establishment of air-flow patterns.

3. The Barcelona Air Quality Campaign

The bulk of the information analyzed during this campaign was acquired with LANL's 1064-nm elastic-backscatter lidar. The experimental methodology used a variety of lidar scans, but this paper focuses on only two scan types: (1) vertical and (2) four-angle correlation.

Vertical scans were acquired by fixing the lidar's azimuth angle and then stepping the elevation angle, θ, through a series of small increments; each elevation angle is separated by a small angle $\Delta\theta$. Vertical scans contain information about the distribution of aerosols in the vertical dimension. A four-angle correlation scan

is acquired by repetitively cycling the lidar through four pairs of azimuth and elevation angles (γ, θ), and is used to determine winds using a best matching scheme between lidar imaged aerosol features, as they travel between different pairs of lidar observation directions (Buttler et al., 2001).

Other measurements included in this study are from soundings (launched each morning at 0600 LST (Local Standard Time, GMT + 2 hours)) and surface meteorological stations. In both cases, monitored variables included temperature, humidity, and wind speed and direction.

During the campaign, the meteorological situation around Barcelona was typical of summertime for the region, i.e., a weak synoptic situation above the Iberian Peninsula. This lack of large-scale forcing allowed the development of mesoscale flows related to the daily heating and cooling cycle. Differential heating of the sea and land establishes sea breezes that generate an on-shore flow during daytime and an off-shore flow during nighttime. At the same time, the mountains (arranged parallel to the coast) cause upslope flows during the day and downslope flows during the night that have the same orientation as the sea/land breeze winds. The orographic features, therefore, enhance the inflow/outflow regime of the sea/land breeze system.

The intense heating above the Iberian Peninsula during this time of year and the lack of synoptic forcings causes a thermal low to develop over the Iberian Peninsula; it is referred to as 'the Iberian thermal low' (Millán et al., 1997). This low-pressure area favors the convergence of air flows towards the centre of the Peninsula and the injection of pollutants into higher levels of the atmosphere, where they are returned to the coast.

4. Vertical Scans

Aerosols travel with the wind, and are considered good tracers of atmospheric movements. Furthermore, because aerosols are emitted in the city together with other pollutants of interest (in processes such as combustion of fossil fuels by cars, which is the main source of air pollution in the city (Costa and Baldasano, 1996)), it is assumed that they will also migrate together (except for gravitational settling of aerosols sized over 1 μm). Because of this, the time evolution of aerosols can be used to monitor the circulation of air pollutants in a study region.

4.1. TIME SERIES ANALYSIS

Analysis of vertical scans of the atmosphere over Barcelona revealed that the transport of aerosols in the region is coupled to sea-breeze circulations and mountain-induced winds. These effects cause a multilayer arrangement of pollutants over the city (Figure 2). The lidar, located at 285-m altitude, was directed towards the sea (direction along vertical scans in Figure 2 is shown in Figure 1).

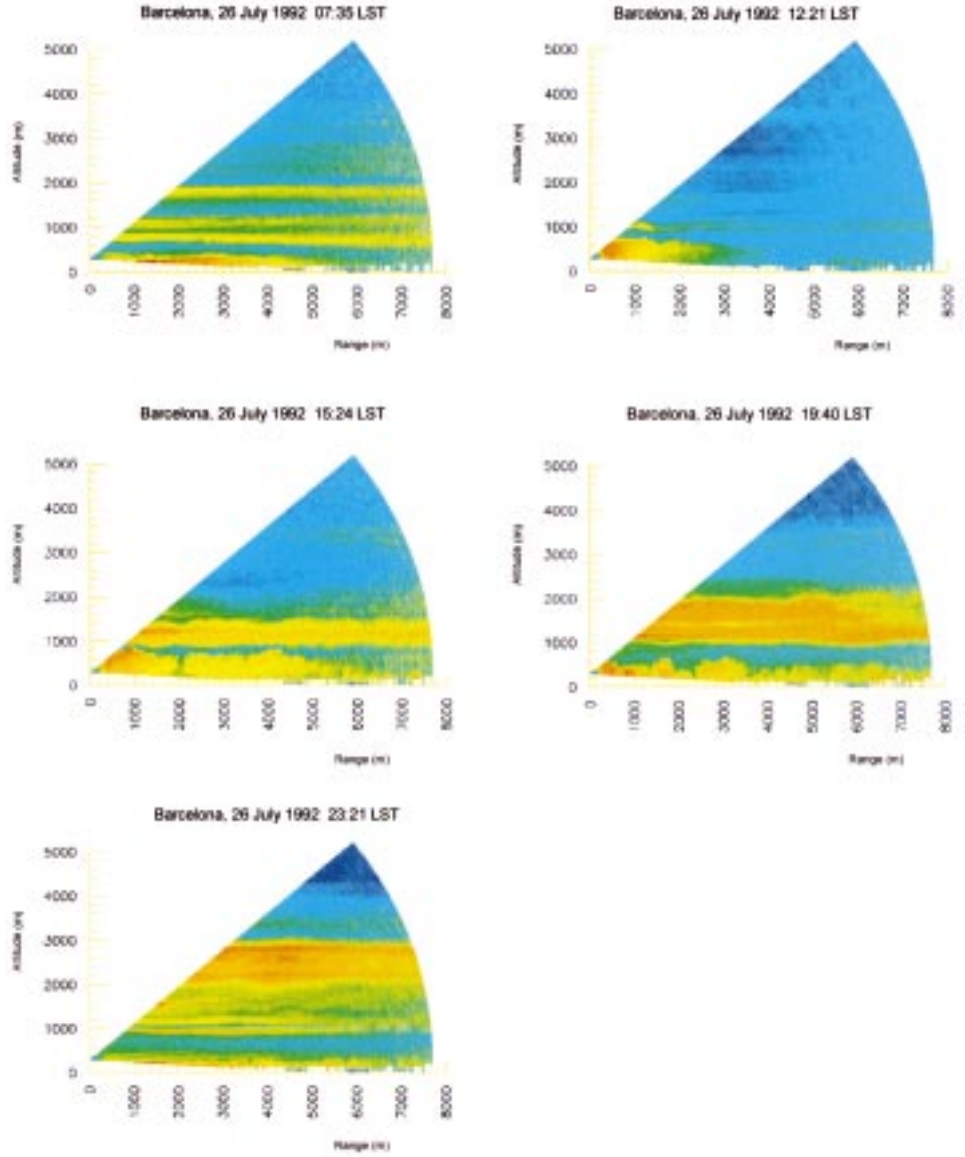

Figure 2. Elastic-backscatter lidar vertical scans (msl) acquired in Barcelona on 26 July 1992 at 0735 LST, 1222 LST, 1524 LST, 1940 LST and 2321 LST. Lidar position was at the origin of coordinates. Red indicates high concentrations of aerosols, whereas blue indicates low concentrations.

Layers form when aerosols are injected into the return flow that completes the sea-breeze circulatory cell. As the day progresses and the breeze penetrates further inland, the circulatory cell associated with it grows, and its associated return flow occurs at higher altitudes. Orographic injections of aerosols from the surrounding mountains are added to this return flow.

Many aerosols are emitted into the atmosphere during the morning (Figure 2). As solar radiation increases, turbulence intensity increases and a mixing layer (ML) forms. Transport and diffusion in the lower atmosphere are highly dependent on the structure of the planetary boundary layer (PBL), and an important feature of the PBL is the depth of the ML (Stull, 1988). Within the ML, scalar passive quantities, such as aerosols, are nearly uniformly mixed. Because aerosols are well mixed within the ML, the lidar images them as a layer of nearly uniform range-corrected backscatter. A sudden decrease in lidar signal is observed above the ML. This decrease coincides with the decrease of aerosols, and thus the transition from dirty to clean air. The ML over land during this time of year in the Barcelona region grows to a maximum height of 800–1000 m at about 1300 LST.

In the afternoon (1524 LST scan) the lidar captured the development of a thermal internal boundary layer (TIBL) (Nakane and Sasano, 1986; Hayden et al., 1997). The TIBL is formed above the terrain, as cool and stable air from the sea flows inland over the heated surface of the land. The formation of the TIBL has been reproduced in a dispersion simulation of CO carried out for one of the days of the campaign in Barcelona (Soriano and Baldasano, 1998) The landward flow causes the formation of an elevated layer of aerosols at about 800 m altitude; aerosols carried aloft by the return flow of the breeze and by forcings caused by the coastal mountain range, feed this elevated layer.

As the afternoon advances, more aerosols are integrated into an additional layer positioned at higher altitudes ($\sim$1500 m). This layer is caused on one hand by the sea-breeze development, whose return flow takes place at higher levels as the day advances, and on the other hand by the frontal penetration of the inland sea breeze as it passes over the coastal mountain range, reaching the pre-coastal mountain range. Return flows from this second mountain range are higher, since the mountains are higher.

In the late evening and early night new elevated layers appear at higher levels (over 3000 m). These layers are believed to be caused by peninsular-scale circulations related to the thermal low that forms above the center of the Iberian Peninsula in summertime (Millán et al., 1997), as discussed in the previous section. General off-shore circulations dissipate aerosol layers during the night, and the remains of elevated layers are still visible in the 0735 LST scan.

4.2. Comparison of vertical scans with radiosonde profiles

According to the description of the aerosol arrangement observed with the lidar, it seems that the different layers of aerosols monitored have experienced different

processes and air masses during their circulation through the atmosphere. This suggests that their physical properties (such as temperature or water content) could have changed along their trajectories.

Several reports have detailed how the aerosol distribution monitored with lidar is strongly correlated with the atmospheric temperature profile (Endlich et al., 1979; Coulter, 1979; Sasano et al., 1982; Van Pul et al., 1994). This is the case of the ML described in Sec. 4.1. The top of a ML is usually capped by a temperature inversion; it forces pollutants emitted at the surface to remain within the ML. In addition, specific humidity is uniform if the atmosphere is well mixed, and water content will differ in the transition from the ML to a different mass of air. Relative humidity profiles are useful in assessing the influence of increased aerosol size caused by water absorption on backscatter signal (Dupont et al., 1994).

Soundings were thus compared with vertical profiles of range-corrected elastic backscatter lidar data. This was accomplished by averaging all range-corrected lidar data within a fixed horizontal range (4200 to 5500 m from the lidar). These averaged data are plotted at the altitudes where radiosonde measurements were available, but only lidar vertical scans acquired at the nearest time to the radiosondes launches (0600 LST) were used. Figure 3 shows an example of a comparison between a lidar vertical scan acquired at 0618 LST on 27 July 1992 to profiles of potential temperature, relative humidity, and specific humidity from a radiosonde launched at 0600 LST.

These plots clearly show that aerosol layers are strongly correlated with layers of different stability. Aerosols are accumulated in the first few hundreds of metres of the atmosphere because the nocturnal surface temperature inversion (potential temperature profile region of strong and positive gradient) prevents aerosols that originated near the surface from moving up. Above this layer, and above an aerosol free region, an elevated aerosol layer is seen between 1250 and 2000 m, a layer with a temperature profile that corresponds to a nearly-neutral atmosphere. Aerosols were trapped in this layer because of the strong stabilization present at its top and bottom, which restricted the vertical dispersion of aerosols trapped in this layer. Aerosols are free, however, to move in the horizontal dimension. Another region of elevated backscatter signal is seen at $\sim$3500 m. This region coincides with a sudden stabilization of the atmosphere, believed to mark the region dominated by the synoptic-scale situation and the transition to the free atmosphere.

If an air mass is well mixed, its corresponding specific humidity profile should be constant with height. Furthermore, because specific humidity is a highly conservative quantity, it can be used to identify air masses of different origin. Water vapor is concentrated in the lower atmosphere mainly due to evaporation from the soil or sea. The lidar also reveals a layer (between 1000 and 2000 m) characterized by an enhanced backscatter signal which coincides with a layer in which the water content is high. The clean air layer between this elevated layer and the surface layer, has a low water content, which confirms that this air is different from that immediately above or below.

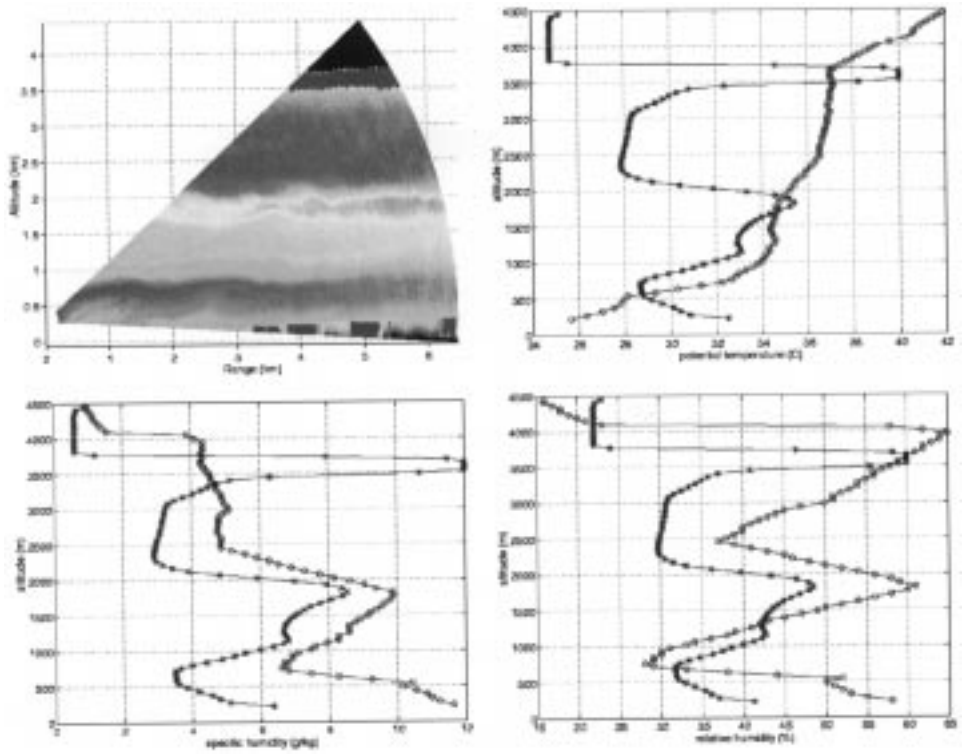

Figure 3. Comparison of lidar vertical scan (msl) in Barcelona on 27 July 1992 at 0618 LST (stars, in arbitrary units) with the vertical profiles (circles) of temperature, specific humidity and relative humidity from a radiosonde launched at 0600 LST. Lighter colours mean higher aerosol content.

Comparison of the lidar profiles and relative humidity profiles showed that, in general, an increase in relative humidity corresponds to an increase in range-corrected backscatter. How aerosols swell with increasing relative humidity has been well documented (Werner, 1972; Dupont et al., 1994, among others). At low relative humidity particles can aggregate molecules of water by adsorption only. At high relative humidity, however, particles grow by absorption of water molecules, increasing their radii, and therefore their backscatter cross-section. According to the high values of relative humidity registered in Barcelona (i.e., because of its seaside location) one can assume that humidity effects can be important on the lidar data through a swelling of the aerosols and an increase of its effective cross-section. This swelling would cause an increase in the backscattered lidar signal that would not correspond to an increase in the concentration of aerosols.

5. Lidar Wind Fields

Remote determination of wind speed and direction with elastic-backscatter lidar techniques relies on the imaging of naturally-occurring aerosol density inhomogeneities (Schols and Eloranta, 1992). Aerosols are efficient tracers of the dynamics and winds, since they respond rapidly to changes in air velocity. The algorithm used for the extraction of the wind information from the lidar signal is based on the maximum cross-correlation technique developed at LANL (Buttler and Eichinger, 1994; Buttler, 1996; Soriano et al., 1997; Buttler et al., 2001). The technique uses images constructed from repetitive laser shots aimed at different points. In the case of the Barcelona field experiment, the sampling pattern consisted of four angles describing a square, a four-angle correlation scan.

Before images are constructed and analyzed, the recorded signal is corrected for the background light (which is constant with range) and for the r^{-2} attenuation of the scattered signal (where r is the range, i.e., the distance from the laser source). Data are then arranged into two-dimensional images, represented as a function of *range* (distance from lidar), and *time* (time of each record). Each time-range image, consisting of a group four observation angles, was then low-pass filtered (to improve the quality of the image) with a two-dimensional (time-space) Gaussian filter, which reduces high frequency fluctuations, or noise, occurring faster than the detector bandwidth of 3 MHz (which placed an upper bound of about 25 m on the minimum range resolution of the lidar). Next, images are processed with the maximum cross-correlation method to determine the winds. This step requires cross-correlation of a subimage (kernel) from one of the lidar observation angles with one of the remaining images, i.e., a distinguishing feature in one time-range image is searched for in another image and assumed to move with the wind. Thus, the maximum value of the cross-correlation between the kernel image and adjacent image gives the time and range lags that are used to calculate the magnitude and direction of the wind (Buttler et al., 2001).

In the Barcelona experiment, the four angles in the scan pattern were separated by 2° in azimuth and elevation. The time required to cycle the lidar 50 times through each of the four pairs of angles was ∼90 seconds (50 times 1.8 s for each cycle). The vertical wind component cannot be determined with the maximum cross-correlation method because mass motions in the vertical direction are usually slower than in the horizontal direction. (Note that in later experiments carried out with LANL's lidar, the scanning pattern was modified to a 3-angle correlation scan where the measurements were acquired over three different azimuth angles and a constant elevation angle, eliminating the possibility of measuring vertical components of the wind.) Thus, in the Barcelona data, cross-correlations were only performed between time-range images acquired at the same elevation angle, to obtain the horizontal wind components.

Velocity vectors measured by the lidar are post-processed to reduce results obtained from false correlations, which mainly occur when the kernel used to obtain

the wind does not contain a well-defined aerosol feature. This happened more than we expected in the analysis of the Barcelona data. For example, many of the 4-angle measurements at Barcelona were acquired at elevation angles of 20° or higher, which in combination with the location of the lidar on a hillside (≈285 m msl), often resulted in a useable range of lidar data 'above the ML', where few aerosol were located. Thus, the maximum cross-correlation technique worked best with lidar data acquired at lower elevation angles over the Llobregat River Valley so that the lidar beam travels through the ML or during the middle of the day when insolation was a maximum and the depth of the ML was greatest. In such cases, convection is fully developed and the lidar is able to monitor the aerosol features produced by the turbulent conditions of the atmosphere.

Finally, wind measurements acquired at similar ranges from the lidar were vector-averaged and their standard deviations calculated. Lidar winds were then compared with radiosonde winds (Buttler et al., 2001), and showed agreement on the order of 1 m s^{-1} in speed and 10° in direction. Similar agreement was found in the 1994 campaign at El Paso, Texas, where lidar winds were compared to Lidar Doppler velocimeter (LDV) winds. These experiments incorporated many lessons learned at Barcelona, leading to a higher density of measurements throughout larger PBL volumes.

Figure 4 shows examples of two-dimensional horizontal winds measured at Barcelona on 28 July 1992 (1330 LST and 2130 LST) from the lidar maximum cross-correlation techniques. The first image corresponds to a typical daytime situation, where southeasterly winds typical of on-shore flows are present, while westerly winds at 2130 LST represent an off-shore situation typical of the nighttime. Other lidar wind measurements are used to evaluate the performance of the meteorological model (Section 7).

6. Numerical Simulation

To complement the information obtained by the lidar numerical simulations were performed with the latest version of the non-hydrostatic meteorological model MEMO (Moussiopoulos, 1994), which includes improved nesting capabilities. MEMO now includes a one-way nesting scheme, in which boundary conditions for an inner grid are obtained from a larger simulation area. Since the lidar wind measurements were restricted to ranges < 5 km, MEMO winds needed to be simulated on a finer scale. However, a bigger domain including all important orographic features was necessary for development of the mesoscale circulations.

The simulation thus incorporated three nested model domains (Figure 5): (1) coarse grid domain covering an area of 80×80 km^2 with a grid resolution of 2×2 km^2, (2) medium grid covering a region of 40×40 km^2 with a 1×1 km^2 mesh, and (3) fine grid (in lidar monitored area) covering 20×20 km^2 with a mesh size of 0.5×0.5 km^2.

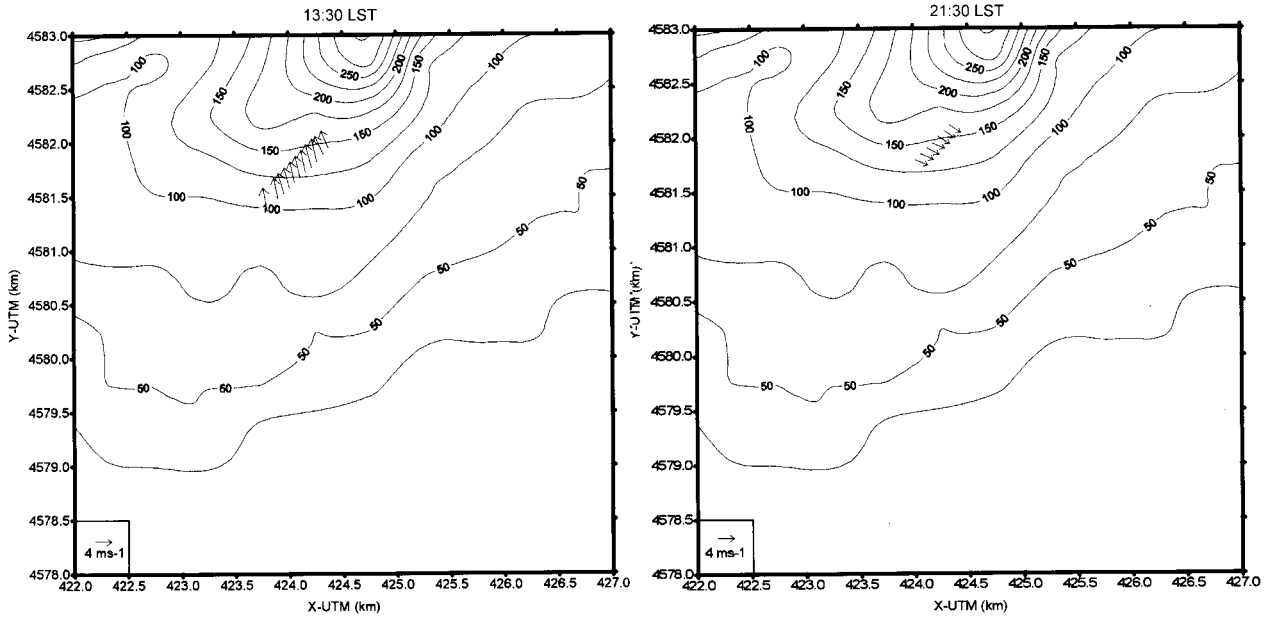

Figure 4. Two-dimensional plots of horizontal winds extracted from the lidar data using the maximum cross-correlation technique at 1330 LST (left) and at 2130 LST (right) on July 28, 1992. See Figure 9 for elevation information.

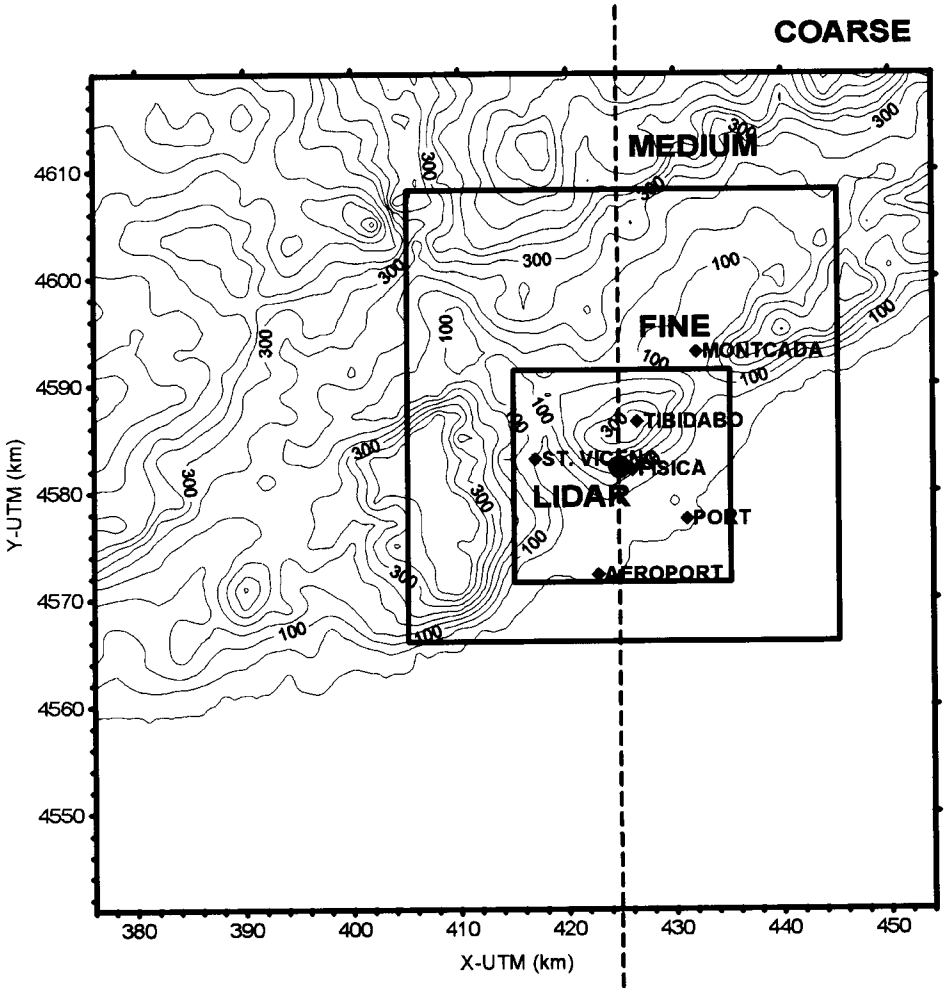

Figure 5. Nested domains for simulation with the meteorological model. Line indicates position of vertical cross-section represented in Figures 7 and 8. Locations of the surface stations used for evaluation of the model in Figure 8 are also included.

The simulated day of interest was 28 July 1992, but the simulation began at 2100 LST the preceding day and ran for 27 hours. Radiosonde data acquired in Barcelona at 0600 LST, supplemented with information from radiosonde launchings at Zaragoza and Palma de Mallorca at 0000 GMT and 1200 GMT, provided the initial state and boundary conditions during the simulation with MEMO.

Two-dimensional slices of the simulated wind fields demonstrate the model's ability to simulate the on-shore and off-shore flows typical of the sea-breeze circulation within the greater Barcelona air basin. Figures 6 and 7 show horizontal cross-sections of winds 10 m above the terrain for the coarse, medium, and fine scale grids, and a north-south vertical cross-section for the coarse domain at

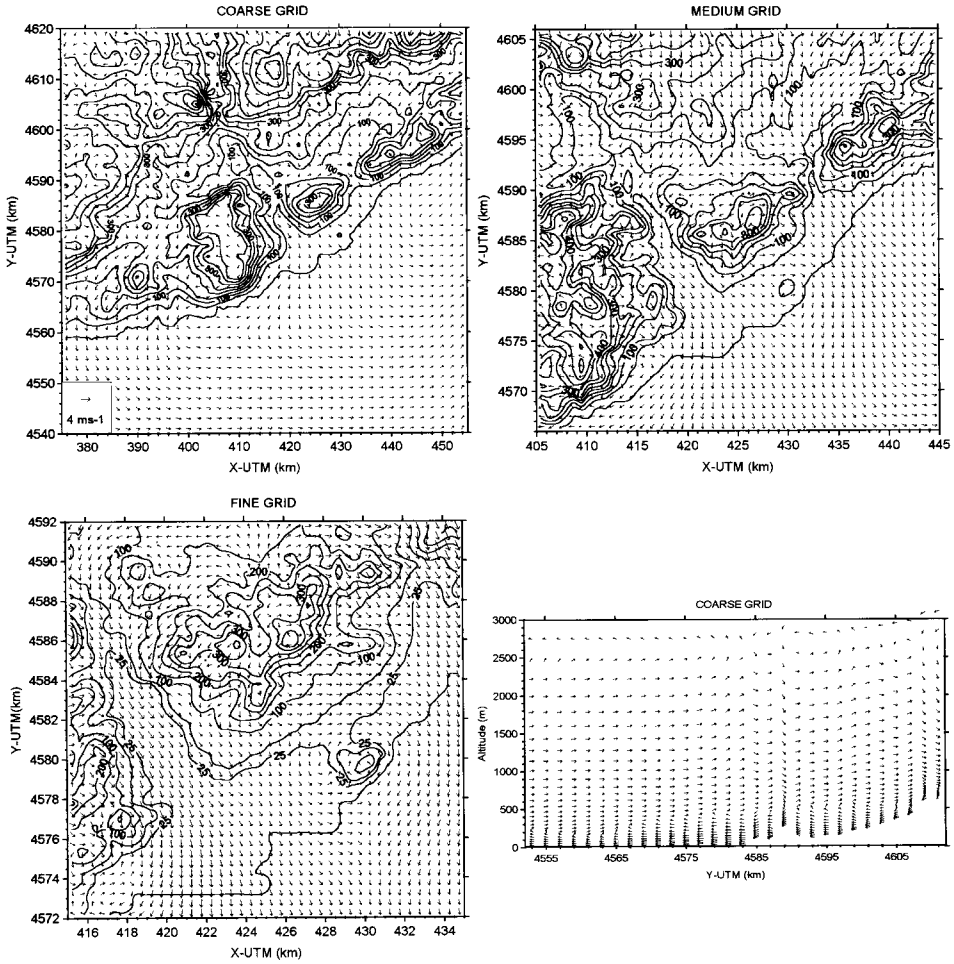

Figure 6. Simulated horizontal cross-sections at 10 m height for the coarse, medium and fine grids, and a north–south vertical cross-section of the wind field, in the plane indicated in Figure 5, at 0500 LST, on 28 July 1992.

0500 and 1600 LST, respectively. The vertical wind component of the vertical cross-sections is enhanced by a factor of 10.

At 0500 LST, the typical nighttime situation is characterized by land-to-sea winds, down-slope winds in the coastal and pre-coastal mountain ranges, and drainage winds in the valleys. Winds are generally weak at this time because the land breeze is usually much weaker than the sea breeze, both in velocity and height, since there is no lower heat source to carry the circulation to greater heights as with the sea breeze. The concurrent cross-section shows winds blowing towards the sea (south) in the first 400 m above the terrain. Winds aloft have a general inland component, in agreement with the geostrophic wind profile imposed on the model.

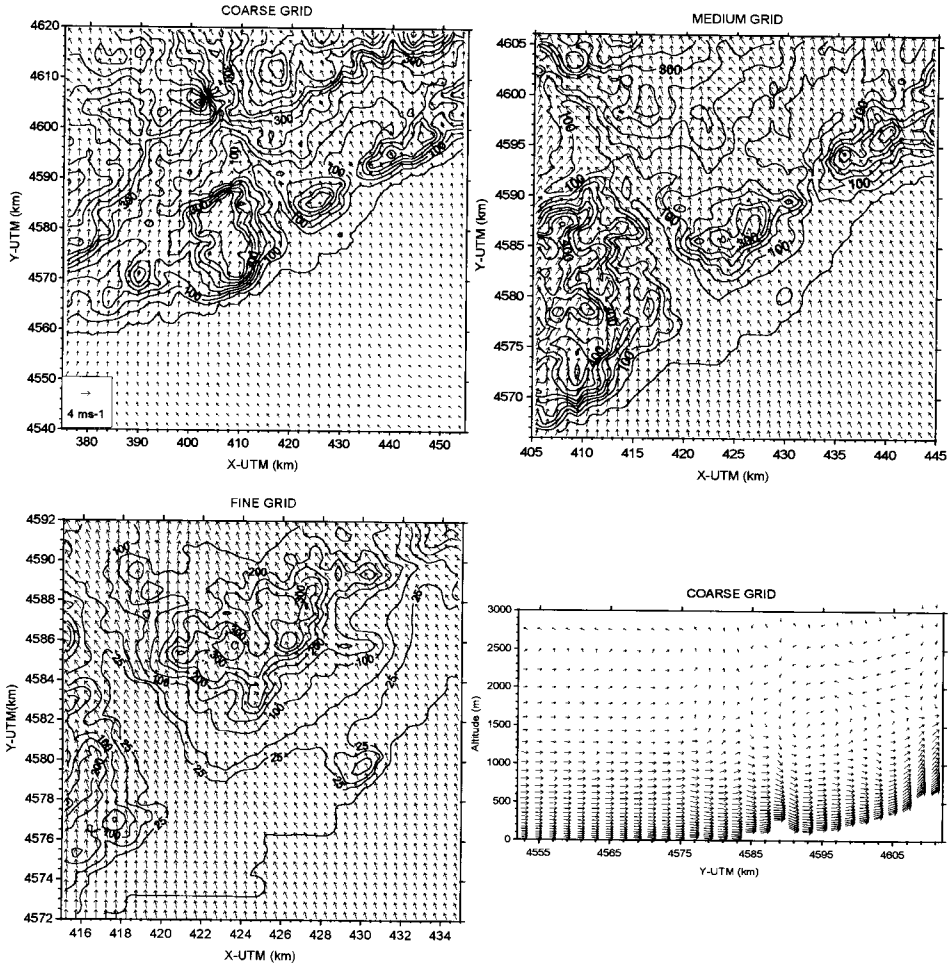

Figure 7. Simulated horizontal cross-sections at 10 m height for the coarse, medium and fine grids, and a north–south vertical cross-section of the wind field, in the plane indicated in Figure 5, at 1600 LST, on 28 July 1992.

The mid-afternoon plots at 1600 LST, however, show the typical daytime wind flow with flows characterized by an onshore sea breeze, up-slope mountain winds, and up-valley winds. The orientation of the mountain ranges parallel to the coastline causes upslope winds in the same direction as the sea-breeze flow, causing strong winds of up to 7–8 m s^{-1}. For these reasons, no sea-breeze front is evident in the two-dimensional wind field plots. However, we can see that winds a few kilometres inland are stronger than the coastal winds, implying that mountain winds are added to the onshore winds generated at the coast.

The concurrent vertical cross-section also shows this general inflow pattern, with stronger winds in a layer 800 to 1000 m above the terrain; this layer corresponds to the sea-breeze inland front. Again, we can see that winds are stronger

above the terrain than above the sea (south in cross-section), at both the coastal and the pre-coastal mountain ranges. At this time of the day, the sea-breeze front has passed over the coastal mountain range and overwhelmed upslope winds in the inner slope of this range. The return wind caused by the orographic injection at the pre-coastal mountain range is seen above 1800 m altitude.

Finally, the simulation in the inner domains allowed us to analyze the wind pattern in the city, and its surrounding mountains and valleys. These analyses show a decreased wind intensity above the urban canopy caused by increased roughness due to the buildings and other man-made roughness features. The channeling of the winds in the valleys and the formation of downslope winds in opposite directions on the opposing slopes of the mountain ranges are both also more evident in the inner domains.

7. Model Performance

The performance of a mesoscale meteorological model is usually determined by comparison of wind simulations in the lowest layer of the domain with measurements from surface stations. Figure 8 shows this type of evaluation for MEMO, i.e., a comparison between fine, medium, and coarse grid simulated winds and those measured at six meteorological surface stations. The graphs show good agreement between the simulated and measured winds, as MEMO accurately predicted the diurnal cycle and timing of the transition from the nighttime to daytime situation. Comparisons for Port and Tibidabo stations are not as satisfactory as the others, especially for wind speed. We believed this is caused by the particular location of these stations. Port is located on the coastline, and Tibidabo is located at the top of the Coastal Mountain Range. Those specific situations might not be well described in their corresponding model cell and cause the disagreements.

The graphs also show that the nested grids with denser meshes do not produce significant improvements in the simulated winds, implying that perhaps the resolution of the orography for the coarse grid is adequate to simulate the main circulatory patterns in the area.

We have used the lidar winds to evaluate MEMO at higher altitudes. This type of comparison is particularly interesting in regions of complex orography, such as Barcelona, with phenomena with an important vertical structure (sea breezes and mountain-related flows). Figure 9 shows a comparison between simulated (fine grid) and lidar winds. Because lidar determined winds are obtained along the line of view of the laser beam, they are represented as a function of ‘range from lidar’, on the x-axis, and ‘msl-altitude’ on the y-axis. The modeled winds correspond to the model cells the laser beam traverses during its travel.

A statistical comparison between the simulated and lidar winds was also performed. Table I shows a comparison between lidar and MEMO winds at 1230 LST. The lidar winds include a deviation, which arises as the value of the lidar-wind

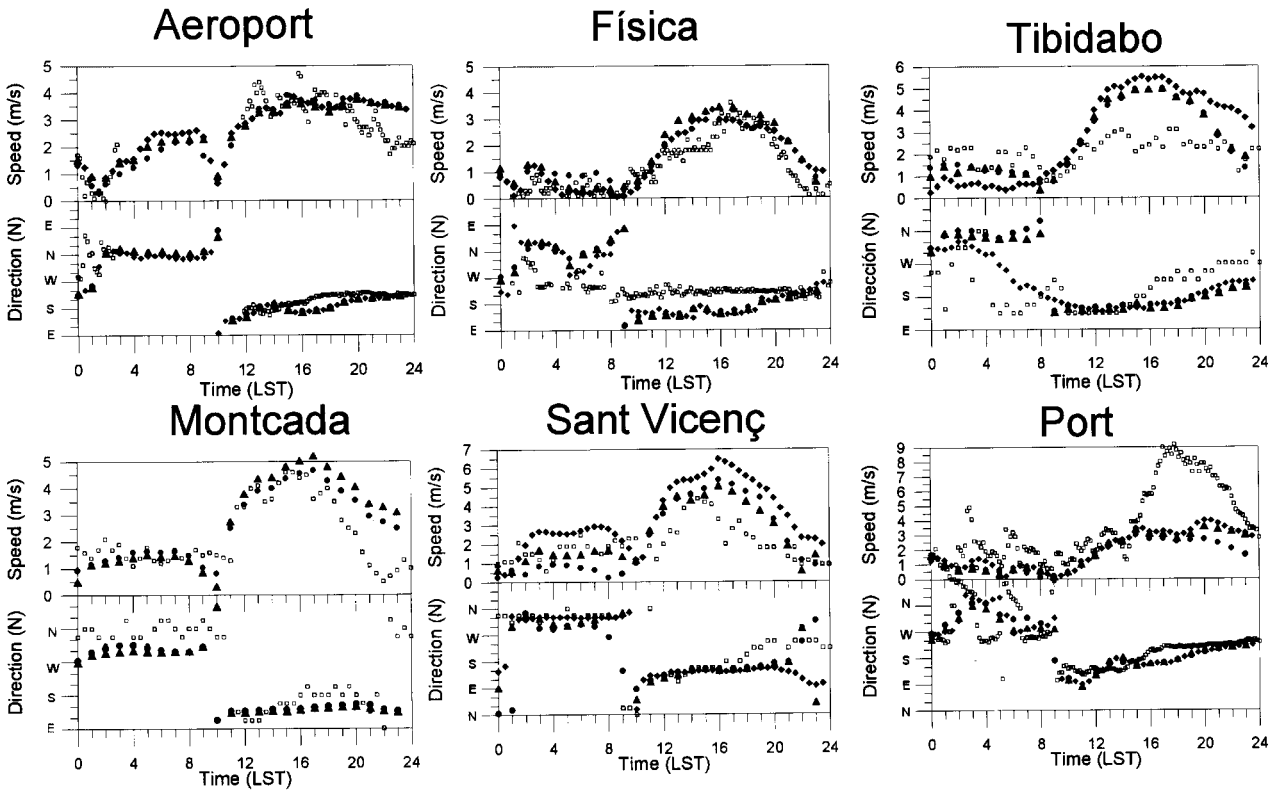

Figure 8. Wind speed and direction calculated by the model for different grids (coarse ●, medium ▲ and fine ♦), compared to surface station measurements □.

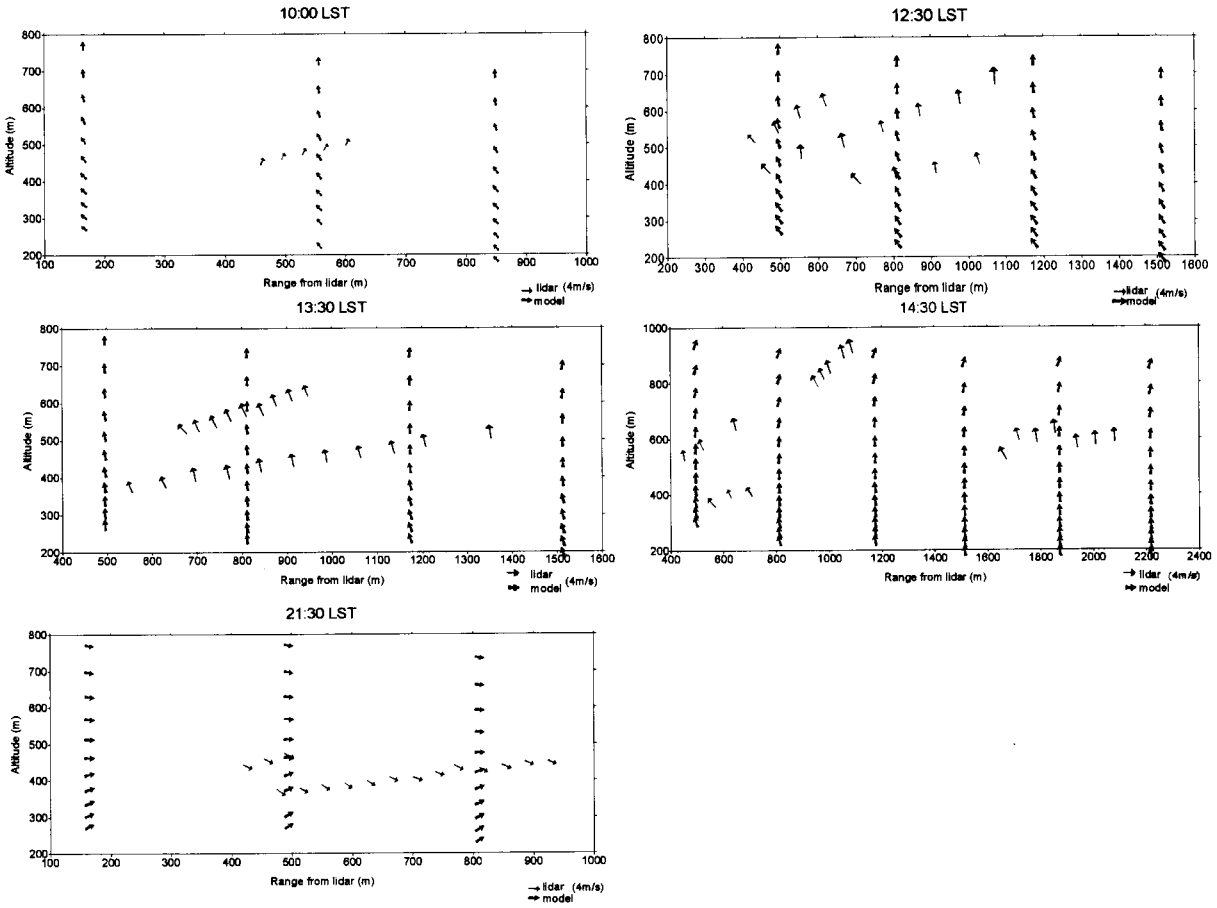

Figure 9. Horizontal wind vectors from the model line grid compared to the lidar winds at 1230 LST on 28 July 1992.

TABLE I

Wind speed (v) and direction (d) measured by lidar and modeled at each model cell the lidar line of view crossed at 1230 LST on 28 July 1992.

Model cell x, y, z	alt (m)	v-lidar (m s^{-1})	d-lidar (deg)	v-model (m s^{-1})	d-model (deg)
[19][20][11]	493.3	3.3 ± 0.5	164.9 ± 5.1	3.2	160.9
[19][20][12]	555.0	3.7 ± 0.6	161.5 ± 6.8	3.2	166.4
[19][20][13]	623.3	3.5 ± 0.6	168.6 ± 8.2	3.3	171.8
[19][20][14]	698.7	4.2 ± 0.6	170.1 ± 6.9	3.4	176.3
[19][21][12]	536.6	4.3 ± 0.4	178.0 ± 6.0	3.3	166.8
[19][21][13]	605.1	3.6 ± 0.7	151.5 ± 10.4	3.3	172.0
[19][21][14]	680.7	4.3 ± 0.8	162.3 ± 7.8	3.5	176.4
Bias/rmse				0.53/0.62	−4.8/10.8

TABLE II

Statistics of the comparison between the lidar-winds and the model-winds for 28 July 1992.

Time (LST)	Speed-bias (m s^{-1})	Speed-rmse (m s^{-1})	dir-bias (deg)	dir-rmse (deg)
1000	−0.01	0.56	53.8	56.2
1230	0.53	0.62	−4.8	10.8
1330	2.15	2.20	−9.4	14.3
1430	1.43	1.95	−12.0	12.3
2130	−0.3	0.3	27.6	27.2

within a certain model cell represents a vector average of all lidar winds within that cell. In addition, two statistics have been calculated for speed and direction: (1) bias, or average differences between observed and modeled values, and (2) root mean squared error (rmse, σ), the square root of average of squared differences. The bias contains information about the model tendency to overpredict or underpredict measurements, while σ gives a measure of the spread of the differences. Table II shows these statistical comparisons for different times.

Tables I and II and plots (Figure 9) demonstrate the accuracy of the simulated winds for Barcelona, because agreement between the lidar and model winds is good. For example, consider the afternoon plots between 1230 and 1430 LST: the model showed a sea-breeze circulation from the southeast which developed from the lower portion of the atmosphere and then simulated the wind shift toward the south-southwest (parallel to the coastline) as the afternoon progressed. This change

is less evident at higher levels, where mesoscale effects are less important. The corresponding statistics for these times show a model tendency to underpredict wind speeds, but to accurately depict the wind direction.

Comparison at 1000 LST (top left in Figure 9) shows the start of a circulation from sea to land in the model while the lidar winds continued to show a land-to-sea component typical of the nighttime regime. We note that it is around this time that the transition between nighttime and daytime situations occurs (note in the graph the low speed of the winds). The results show that the model computed the sea-to-land breeze transition typical of the daytime regime too early. At this transition time the model correctly predicted the low speeds typical of these period but not the direction. However, the model also correctly reproduced the land breeze with a westerly component that started to develop at 2100 LST (bottom left plot in Figure 9), in the transition from the daytime to the nighttime regime.

8. Conclusion

Information from the lidar and the wind fields calculated by the MEMO model is used to describe the circulatory patterns of air pollutants in the Barcelona Air Basin. Figure 10 shows schematics of the mechanisms determined as important in the development of atmospheric circulatory patterns within the Basin for a typical summertime situation.

The first mechanism is for the typical midday to early afternoon situation, characterized by sea-breeze inland flows, upslope winds in the mountain ranges, and up-valley winds in the river valleys. Return flows from the sea-breeze circulatory cell and from the orographic injection of the mountains of the coastal range take place between 1000–2000 m, dependent on the depth of development of the circulation cell. The high altitude situation is dominated by a general subsidence caused by the high-pressure area located above the region at the synoptic scale.

The mid-afternoon situation also shows a general inflow circulation typical of the daytime period. However by this time, the sea breeze has penetrated over the coastal mountains and its associated front has reached the pre-coastal mountain range. In addition, return flows produced by orographic injections of this second higher mountain range are situated at higher altitude, above 2500 m. Subsidence persists aloft.

The final situation corresponds to the nighttime regime, i.e., the sea breeze has reversed and a general offshore flow is now present. This offshore flow is characterized by the combined effects of land breeze, drainage valley winds, and downslope winds in the mountains. Subsidence persists on the synoptic scale, and effects from peninsular-scale phenomena are now more evident. As a consequence of the Iberian thermal low centered on the peninsula at this time of the year, pollutants from its centre rise up and then diverge toward the coast during nighttime. This return flow takes place at even higher altitudes (> 4000 m) and explains the

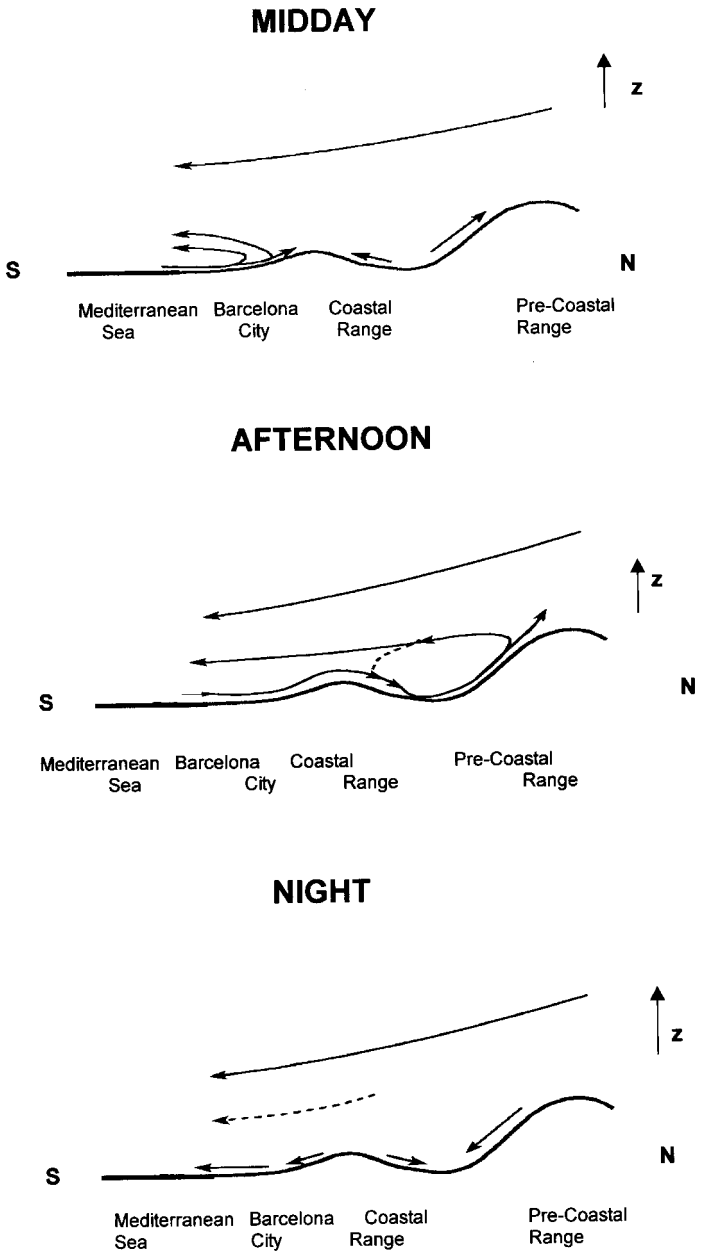

Figure 10. Schematic vertical cross-sections of atmospheric circulations in the Barcelona Air Basin during a typical summer day during midday, afternoon and night periods.

elevated aerosol layers imaged by the lidar during the night and early morning scans. Their reproduction by MEMO would require an additional peninsular-scale simulation domain.

This work thus demonstrates the suitability of combining lidar techniques with meteorological mesoscale models to study atmospheric circulations and boundary-layer structure at a regional to local scale. The high dependence of the atmospheric circulation at this range on the particular characteristics of the terrain makes both approaches appropriate for these kinds of studies. The high-resolution remotely measured data acquired with the lidar and the possibility to simulate the atmospheric situation with a meteorological model, allows a wider view of the phenomena that takes place in a study area. This perspective is lost when only one of the approaches is applied – either an experimental or numerical approach.

Finally, one of the main contributions of the proposed methodology to the field of atmospheric modelling comes from the ability of the lidar to remotely determine three-dimensional fields of horizontal winds. This capability allows the evaluation of models with height, where 'local' effects that measurements from surface stations might include are minimized. However, only comparison in the downwind range of the sea breeze were possible, since for this experiment lidar wind measurements were only available in this range.

Acknowledgements

We extend our appreciation to all the people who participated in some way in the acquisition of the experimental data analyzed in this study. Our thanks to the personnel from Los Alamos National Laboratory who operated the lidar system. Thanks are due to the Instituto Nacional de Meteorología for providing the radiosonde data and to the Ajuntament de Barcelona and the Àrea Metropolitana de Barcelona for providing the measurements from the surface meteorological stations.

Thanks to CESCA (Centre de Supercomputació de Catalunya) for allowing use of their supercomputers to run the meteorological model and to the Departament de Medi Ambient de la Generalitat de Catalunya and the CICYT (Comisión Interdepartamental de Ciencia y Tecnología, grant AMB96-1144-CO2) for funding part of this work.

Cecilia Soriano specifically acknowledges Prof. Robert Bornstein, from San Jose State University, San Jose, California, for his useful comments and suggestions during the completion of this study; Douglas Alde, from Los Alamos National Laboratory, for his assistance in programming; and Michael Brown, also from Los Alamos National Laboratory, for reviewing the manuscript and adding useful comments.

References

Baldasano, J. M., Cremades, L., and Soriano, C.: 1994a, 'Circulation of Air Pollutants over the Barcelona Geographical Area in Summertime', in G. Angeletti and G. Restelli (eds.), *Proceedings of the Sixth European Symposium on Physico-Chemical Behavior of Atmospheric Pollutants*, Environmental Research Program of the European Community, Air Pollution Research Report EUR 15609/1, 474–479.

Baldasano, J. M., Costa, M., Cremades, L., Flassak, Th., and Wortmann, W.: 1994b, 'Air Quality Simulation in the Barcelona Geographical Area for a Typical Summer Day', in N. Moussiopoulos (ed.), *The EUMAC Zooming Model: Model Structure and Applications*, EUROTRAC-155, Garmish-Patenkirchen, pp. 87–103.

Buttler, W. T.: 1996, 'Three-Dimensional Elastic Lidar Winds', *Eighteen International Laser Radar Conference*, Berlin, Germany, 22–26 July, 1996, in A. Ansmann et al. (eds.), *Advances in Atmospheric Remote Sensing*, Springer-Verlag, pp. 271–274.

Buttler, W. T. and Eichinger, W. E.: 1994, 'Wind-Speed Measurements with a Scanning Elastic-Backscatter Lidar, in *Proceedings of the 21st Conference on Agriculture and Forest*, San Diego, California, March 7–11, American Meteorological Society.

Buttler, W. T., Nickel, G. H., Soriano, C., and Baldasano, J. M.: 2001, 'Remote Sensing of Three-Dimensional Winds with Elastic Lidar: Explanation of Cross-Correlation Method', *Boundary-Layer Meteorol.*, in press.

Calbó, J. and Baldasano, J. M.: 1995, 'PROMETEO: An Hydrostatic Mesoscale Model Applied to the Simulation of Land-Sea Breeze in the Barcelona Area', *Env. Soft.* **10**, 139–155.

Costa, M. and Baldasano, J. M.: 1996, 'Development of a Source Emission Model for Atmospheric Pollutants in the Barcelona Area', *Atmos. Environ.* **30A**, 309–318.

Coulter, R. L.: 1979, 'A Comparison of Three Methods for Measuring Mixing-Layer Height', *J. Appl. Meteorol.* **18**, 1495–1499.

Dupont, E., Pelon, J., and Flamant, C.: 1994, 'Study of the Convective Boundary-Layer Structure by Scattering Lidar', *Boundary-Layer Meteorol*. **69**, 1–25.

Endlich, R. H., Ludwig, F. L., and Uthe, E. E.: 1979, 'An Automatic Method for Determining the Mixing Layer Depth from Lidar Observations', *Atmos. Environ*. **13**, 1051–1056.

Hayden, K. L., Anlauf, K. G., Hoff, R. M., Strapp, J. W., Bottenheim, J. W., Wiebe, H. A., Froude, F. A., Martin, J. B., Steyn D. G., and McKendry, I. G.: 1997, 'The Vertical Chemical and Meteorological Structure of the Boundary Layer in the Lower Fraser Valley during Pacific'93', *Atmos. Environ.* **31**, 2089–2105.

Johnson, W. B.: 1969, 'Lidar Applications in Air Pollution Research and Control., *J. Air. Pollut. Control Assoc*. **19**, 176–180.

Hoff, R. M., Harwood, M., Sheppard, A., Froude, F., Martin, J. B., and Strapp, W.: 1997, 'Use of an Airborne Lidar to Determine Aerosol Sources and Movement in the Lower Fraser Valley (LFV), BC', *Atmos. Environ.* **31**, 2123–2134.

Millán, M., Salvador, R., and Mantilla, E.: 1997, 'Photooxidant Dynamics in the Mediterranean Basin in Summer: Results from European Research Projects', *J. Geophys. Res.* **102**, 8811–8823.

Moussiopoulos, N.: 1994, 'MEMO-A Non-Hydrostatic Mesoscale Model', in N. Moussiopoulos (ed.), *The EUMAC Zooming Model: Model Structure and Applications*, EUROTRAC-155, Garmish-Partenkirchen, pp. 7–22.

Nakane, H. and Sasano, Y.: 'Structure of the Sea-Breeze Front Revealed by Scanning Lidar', *J. Meteorol. Soc. Jap.* **64**, 787–792.

Sasano, Y., Shigematsu, A., Shimizu, H., Takeuchi, N., and Okuda, M.: 1982, 'On the Relationship between the Aerosol Layer Height and the Mixed Layer Height Determined by Laser Radar and Low-Level Radiosonde Observations', *J. Meteorol. Soc. Jap.* **60**, 889–895.

Schols, J. L. and Eloranta, E. W.: 1992, 'Calculation of Area-Averaged Vertical Profiles of the Horizontal Wind Velocity from Volume-Imaging Lidar Data', *J. Geoph. Res.* **97**, 18,395–18,407.

Soriano, C.: 1997, *Estudio de las circulaciones atmosféricas en la mesoscala mediante técnicas lidar y simulación numérica: Aplicación al área de Barcelona en una situación de verano*, Ph. D. Thesis, Universitat Politècnica de Catalunya, Barcelona, Spain.

Soriano, C. and Baldasano, J. M.: 1998, *Study of the Land-Sea Interface in the Barcelona Area with Lidar Data and Meteorological Models*, in C. A. Brebbia (ed.), *Environmental Coastal Regions*, Computational Mechanics Publications, pp. 135–142.

Soriano, C., Baldasano, J. M., and Buttler, W. T.: 1997, 'On the Application of Meteorological Models and Lidar Techniques for Air Quality Studies at a Regional Scale', *22nd NATO/CCMS Meeting on Air Pollution Modeling and its Application*, Clermont-Ferrand, France, 2–6 June 1997, in: S. E. Gryning and N. Chaumerliac (eds.), *Air Pollution Modeling and its Application XII*, Plenum Press, pp. 591–600.

Stull, R. B.: 1988, *An Introduction to Boundary Layer Meteorology*, Kluwer Academic Publishers, Dordrecht, 666 pp.

Van Pul, W. A. J., Holstag, A. A. M., and Swart, D. P. J.: 1994, 'A Comparison of ABL Heights Inferred Routinely from Lidar and Radiosondes at Noontime', *Boundary-Layer Meteorol.* **68**, 173–191.

Wakimoto, R. M. and McElroy, J. L.: 1986, 'Lidar Observation of Elevated Pollution Layers over Los Angeles', *J. Clim. and App. Meteorol.* **25**, 1583–1599.

Werner, C.: 1972, 'Lidar Measurements of Atmospheric Aerosol as a Function of Relative Humidity', *Opto-elect.* **4**, 125–132.